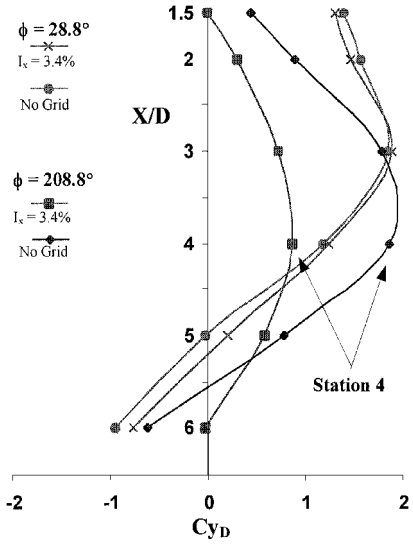


**Fig. 3 Local side-force distributions in the model axial direction when no grid was installed and when $I_x = 0.034$; $\phi = 28.8$ and 208.8 deg.**

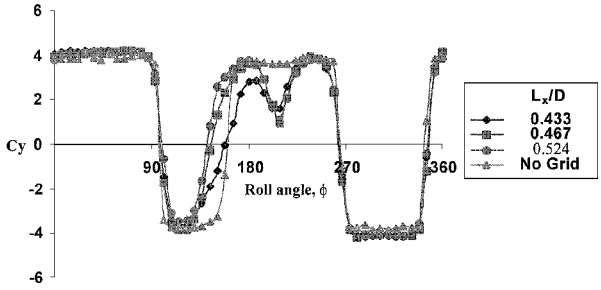


**Fig. 4 Effects of varying the turbulence length scale $L_x$ when turbulence intensity $I_x$ is kept constant at 3.9%.**

direction of the model for cases with and without the presence of the grids. The local side force $Cy_D$ is obtained by integrating the local surface-pressure measurements. Using the results of the turbulence intensity $I_x = 3.4\%$ as an example, it can be seen that at $\phi = 28.8$ deg there is only a very small difference in the local side-force distribution between the relatively smooth (no grid installed) and the turbulent ($I_x = 3.4\%$) flow. This is consistent with the total side-force data shown in Fig. 2. However at $\phi = 208.8$ deg, where there is a large "dip" in the overall side-force distribution in Fig. 2, the turbulence intensity has certainly caused a substantial reduction in the local side force.

We next study the effects of turbulence length scale while keeping the turbulence intensity constant, and the results for the fixed turbulence intensity $I_x$ of 3.9% are shown in Fig. 4. Unfortunately, because of the relatively small range in $L_x/D$ used (0.433–0.524), no clear trend in the change of the side-force distribution with variation in the turbulence length scale can be detected. For the present results the smallest length scale of $L_x/D = 0.433$ appears to have the greatest influence in reducing side force in virtually all cases when $\phi = 208.8$ deg (the approximate roll angle where the greatest side-force reduction takes place). It is believed that a larger range of $L_x/D$ is needed before its effects on the side force can be fully appreciated, and more systematic work is obviously required.

## Conclusions

The effects of freestream turbulence on the side force acting on an ogive cylinder at high angle of attack have been studied experimentally over a range of turbulence intensity and length scale. By carefully locating the positions of the turbulence generating grids upstream of the cylinder, the turbulence intensity was varied independently of the turbulence length scale and vice versa.

Side-force and surface-pressure measurements clearly show that, for a fixed angle of attack, an increase in the turbulence intensity can cause the side force to either decrease or increase, depending on the roll-angle position (surface conditions) of the cylinder. This explains the sometimes contradictory findings reported in the literature. As for the turbulence length scale, it also appears to have influence on the cylinder's side force, but because of the relatively small $L_x/D$ range used no clear trend was detected. In the present case the smallest $L_x/D (= 0.433)$ appears to have the greatest influence in reducing side force. More systematic investigation is needed in this area.

## References

[1]Lamont, P. J., and Hunt, B. L., "Pressure and Force Distributions on a Sharp-Nosed Circular Cylinder at High Angles of Inclination to a Uniform Subsonic Stream," *Journal of Fluid Mechanics*, Vol. 76, No. 3, 1976, pp. 519–559.

[2]Hunt, B. L., and Dexter, P. C., "Pressure on a Slender Body at High Angle of Attack in a Very Low Turbulence Level Air Stream," CP 247, AGARD, Oct. 1978.

[3]Howard, R. M., Rabang, M. P., and Roane, D. P., Jr., "Aerodynamic Effects of a Turbulent Flowfield on a Vertically Launched Missile," *Journal of Spacecraft*, Vol. 26, No. 6, 1989, pp. 445–451.

[4]Wardlaw, A. B., and Yanta, W. J., "Multistable Vortex Patterns on Slender, Circular Bodies at High Incidence," *AIAA Journal*, Vol. 20, No. 4, 1982, pp. 509–515.

[5]Luo, S. C., Lim, T. T., Lua, K. B., Chia, H. T., Goh, E. K. R., and Ho, Q. W., "Flowfield Around Ogive/Elliptic-Tip Cylinder at High Angle of Attack," *AIAA Journal*, Vol. 36, No. 10, 1998, pp. 1778–1787.

[6]Lamont, P. J., "Pressure Around an Inclined Ogive Cylinder with Laminar, Transitional, or Turbulent Separation," *AIAA Journal*, Vol. 20, No. 11, 1982, pp. 1492–1499.

A. Plotkin
*Associate Editor*

# Turbulence in Wake of a Self-Propelled Body with and without Swirl

A. I. Sirviente*
*University of Michigan, Ann Arbor, Michigan 48109-2145*
and
V. C. Patel†
*University of Iowa, Iowa City, Iowa 52242-1585*

## I. Introduction

In the wake of a self-propelled body, the drag of the body is matched by the thrust developed by the propulsion device, and there is no net momentum flux. Measurements in such a momentumless wake of a bluff axisymmetric body propelled by a jet, without[1] and with swirl,[2] were recently made to document the turbulent mixing in the near field and study evolution of the wake. Measurements were also made in so-called component flows, namely the drag wake[3] of the body without propulsion and an isolated nonswirling jet and a swirling jet issuing from the base of the body. The previous publications reported the streamwise development of the momentumless wake, without[1] and with swirl.[2] This development takes place in three stages: the near field, in which the body boundary layer and the jet are clearly evident; an intermediate region, in which the two flows mix up to the axis of the body; and last the

Received 20 December 2000; revision received 30 August 2001; accepted for publication 5 September 2001. 

*Assistant Professor, Department of Naval Architecture and Marine Engineering. Member AIAA.

†Director and Professor, Iowa Institute of Hydraulic Research and Department of Mechanical Engineering. Associate Fellow AIAA.

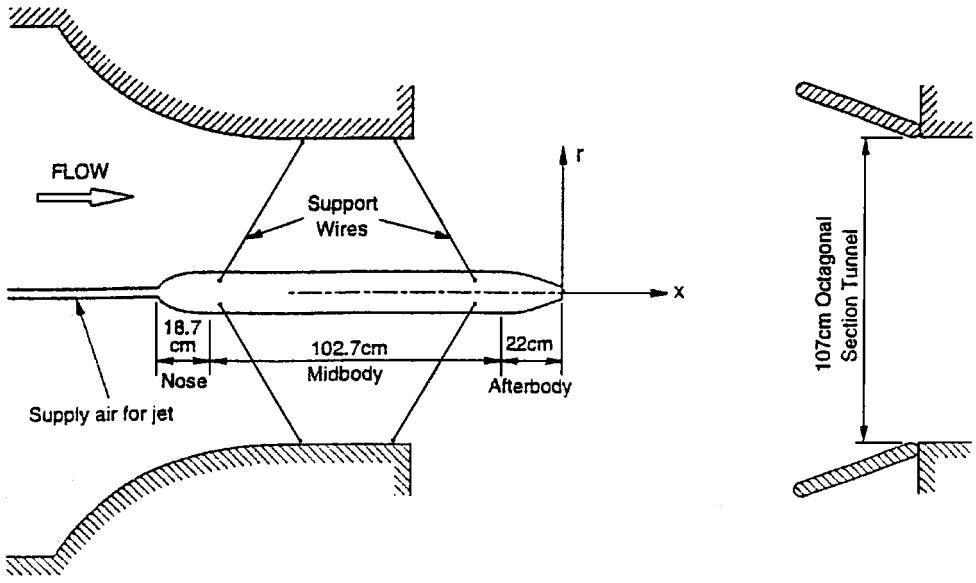


**Fig. 1 Model and tunnel arrangement.**

region of a single shear flow, the developed wake, in which the data reveal varying levels of similarity. The purpose of this Note is to present comparisons of some additional flow characteristics in the third region, the fully mixed wake. Here we consider the distributions of eddy viscosity, intermittency, triple velocity products, and length scales that shed light on the differences in the turbulence.

The experiments were conducted in the 1.07-m octagonal, open test-section, return-circuit wind tunnel of the Iowa Institute of Hydraulic Research. Figure 1 shows the wind tunnel and model along with the coordinate system $(x, r, \theta)$ used to report the data. The freestream velocity $(U_0)$ was set at 16.5 m/s, resulting in a Reynolds number based on the body length (143.45 cm) of $1.58 \times 10^6$. The jet Reynolds number based on the diameter of the jet $(D = 3.90\ \text{cm})$ and the jet maximum axial velocity $(2U_0)$ was $8.6 \times 10^4$. The maximum swirl velocity at the jet exit was $0.95U_0$. A detailed description of the experimental equipment, instrumentation, and measurement procedures can be found in Sirviente and Patel,[1–3] along with an analysis of the uncertainty in the data [2% for the mean velocity components $(U, V, W)$ and 10% for $\overline{uu}$ and $\overline{uv}$ and 20% for the rest of the Reynolds stresses].

In the analysis of conventional wakes with momentum deficit, the centerline velocity $U_c$ is chosen as the velocity scale, and the length scale $b$ is taken as the half-radius based on the mean velocity profile. For momentumless wakes a length scale based on the mean velocity profile is difficult to determine from experimental data because the velocity defect and excess tend to flatten the profile in the fully mixed wake. Therefore, here it is taken as $b_{\overline{uu}_{m/2}}$, namely, the radius where the streamwise Reynolds stress $\overline{uu}$ is one-half of its maximum value. These velocity and length scales are used to nondimensionalize and compare data from different flows.

## II. Eddy Viscosity

If isotropy of the eddy viscosity $\nu_t$ is assumed and thin shear layer approximations are made, $\nu_t$ can be determined from the measured shear stress and gradient of the axial velocity component as

$$\frac{\nu_t}{U_c b} = \frac{-\overline{uv}/U_c^2}{\partial(U/U_c)/\partial(r/b)}$$

The distributions of $\nu_t/U_c b$ in the three flows (i.e., drag wake and momentumless wakes with and without swirl) at station $x/D = 19.53$ are plotted in Fig. 2. Differences in eddy viscosity are of course reflected in the growth and decay rates of these shear flows. It was shown[2] that the mean shear and turbulent shear stress decay very rapidly in the momentumless wake with swirl. This results in larger scatter and uncertainty in the eddy viscosity for that flow. Nevertheless, from Fig. 2 it is seen that the eddy viscosity in

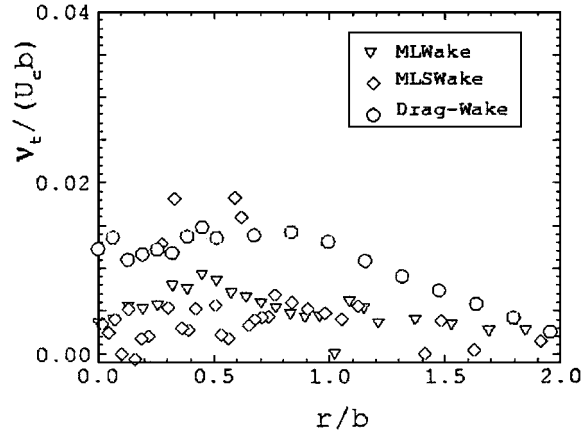


**Fig. 2 Eddy viscosity distribution at station $x/D = 19.53$, in the drag wake and momentumless wakes with and without swirl.**

the momentumless wake without swirl is almost constant around 0.007 and about one-half of the average value in the drag wake, which is 0.012. The average value of the eddy viscosity is reduced in the momentumless swirling wake with a value around 0.005. It can be concluded that swirl tends to reduce the eddy viscosity and therefore the radial transport of axial momentum.

## III. Triple Velocity Correlations

The divergence of the triple velocity correlations comprises the turbulence diffusion terms in the Reynolds-stress transport equations. Thus, for example, the turbulent diffusion of turbulence kinetic energy in the radial direction is given by the radial derivatives of the correlations $\overline{vu^2}$, $\overline{v^3}$, and $\overline{vw^2}$, and these are the only terms retained following thin shear layer approximations. Although the present data are not complete enough to construct the balance of either the turbulence kinetic energy or the component stresses, profiles of the triple products are of interest in identifying differences in turbulent diffusion.

Radial profiles of two correlations appearing in the turbulence kinetic energy equation, namely, $\overline{u^2 v}$ and $\overline{v^3}$, at station $x/D = 19.53$ are shown in Figs. 3a and 3b, respectively. The radial gradients of these represent the radial transport of $\overline{uu}$ and $\overline{vv}$, respectively. Important differences are observed in the shape, slope, and magnitudes among the three flows. The drag (bare-body) wake shows negative values in the vicinity of the centerline indicating a gain of energy by diffusion (from the region of maximum turbulence kinetic energy, which is not at the centerline[3]). In both momentumless wakes,

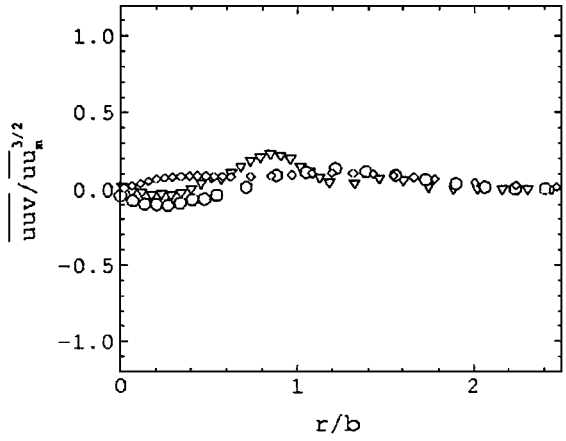


**Fig. 3a Triple velocity correlations at station $x/D = 19.53$, in the drag wake and momentumless wakes with and without swirl.**

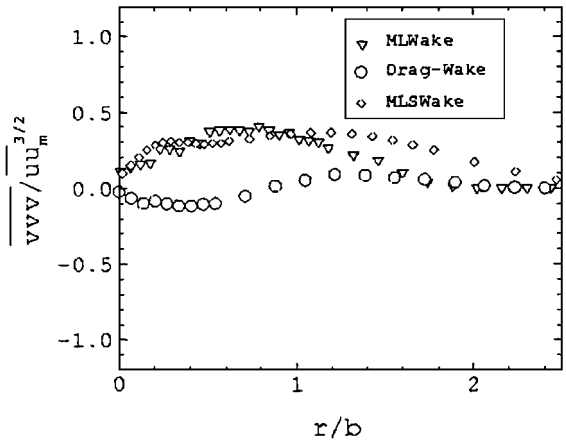


**Fig. 3b Triple velocity correlations at station $x/D = 19.53$, in the drag wake and momentumless wakes with and without swirl.**

on the other hand, diffusion is considerably stronger and radially outward across the flow. The triple correlation measurements thus support the assumption that production of turbulence energy in the momentumless wakes is small, and there exists a balance between diffusion and convection. The effect of swirl is clear in $\overline{u^2 v}$, while $\overline{v^3}$ shows none in the inner region. Although other triple correlations were measured in the experiments, they are not presented here.

## IV. Intermittency

Intermittency $\gamma$ is defined as the fraction of time during which the flow is turbulent. It can be calculated from the flatness factor $F$ of a turbulent signal (of $u$, $v$, $w$, etc.) as $\gamma = F|_0/F$, where the numerator is the flatness where the flow is fully turbulent. Intermittency is closely associated with the process of entrainment and the radial extent of intermittent flow with the size of the large eddies in the flow.

Intermittency distributions at $x/D = 19.53$ calculated from measurements of the axial velocity fluctuation $u$ are compared in Fig. 4. In all three flows there is intermittency beyond a central core, $r/b$ or $r/b_{\overline{uu}_m/2} < 0.6$, say, but the radial location of $\gamma = 0.5$ is quite different. The intermittent region was found to be relatively narrow in the isolated nonswirling jet (not shown), indicating smaller eddies. Tennekes and Lumley[4] reason that this is because the momentum transported by the longitudinal flow is as much as that carried by the transverse flow, implying a compression of eddies in the cross-stream direction. This is not the case in wakes, although the intermittent region in the momentumless wake is narrower than that of the drag wake, implying smaller eddies and reduced entrainment (the measured entrainment was zero, as required by similarity theory). Further correlations with eddy sizes and entrainment are speculative, at best, in view of the uncertainty of the relevance of the length scale used here in the outer region of the momentumless wake.[1,2]

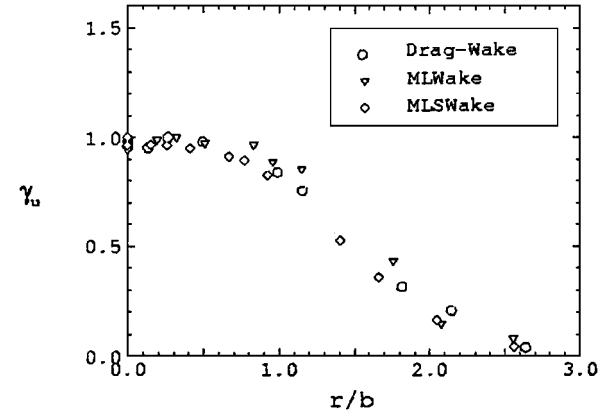


**Fig. 4 Intermittency distribution at station $x/D = 19.53$, in the drag wake and momentumless wakes with and without swirl.**

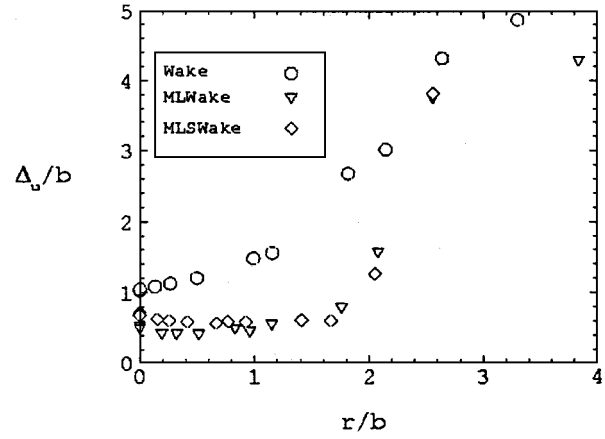


**Fig. 5a Integral length scales at station $x/D = 19.53$, in the drag wake and momentumless wakes with and without swirl.**

More careful consideration of the flow structure in the outer region is necessary to address these issues. The data show practically no difference in the three wakes, while the intermittent flow region in the isolated swirling jet (not shown) was found to be narrower than in the wakes.

## V. Turbulence Length Scales

Two commonly used turbulence length scales were determined from the data. The integral length scale was determined from the measured integral timescale using the Taylor hypothesis. Although the hypothesis applies strictly to homogeneous turbulence, it is often used[5] in other flows where the following conditions apply: $|U(\partial U/\partial x)| \gg |V(\partial U/\partial r)|$ and $\overline{uu}/U^2 \ll 1$. These are satisfied at $x/D = 19.53$ in the three flows under consideration here.

The autocorrelation of the axial velocity fluctuation is $R_{11\tau}(\tau) = \overline{u(t)u(t+\tau)}/\overline{u(t)^2}$, where $t$ is time and $\tau$ is the delay time. Its integration

$$\zeta = \int_0^\infty R_{11\tau}(\tau)\,\mathrm{d}\tau$$

gives the integral timescale $\zeta$, and the integral length scale follows from the Taylor hypothesis $\Delta = U\zeta$. Numerical integration was used to obtain the area under the autocorrelation curve with a cutoff of $10^{-4}$ to ensure convergence of the integral.

Figure 5a shows the integral length scales in the three flows. The largest values of $\Delta$ are found in the drag wake, confirming the observations about eddy sizes from the intermittency distributions. At the centerline $\Delta$ is of the order of the half radius of the drag wake, whereas it is only 0.5b in the momentumless wake without swirl. Swirl tends to increase the integral length in the inner region ($r/b < 1$, say) of the momentumless wake. The distribution of $\Delta$ in the momentumless wake without swirl is very similar to that in the

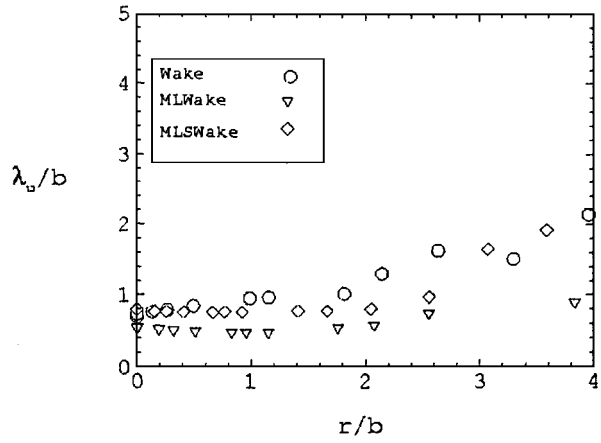


**Fig. 5b Taylor length scales at station $x/D = 19.53$, in the drag wake and momentumless wakes with and without swirl.**

isolated jet (not shown) up to a radial distance of the order $b$, indicating a jet-like flow structure in the central part of the momentumless wake even at this large distance from its origin.

It is generally assumed that at large Reynolds numbers the dissipating eddies are isotropic and the Taylor microscale $\lambda$ can be expressed in terms of the energy dissipation rate $\varepsilon$, as[4] $\varepsilon = 15\nu\overline{uu}/\lambda^2$, where $\nu$ represents the kinematic viscosity of the fluid. The dissipation rate was determined from the isotropic expression and the Taylor hypothesis as $\varepsilon = 15\nu(\partial u/\partial x)^2 = (15\nu/U^2)(\partial u/\partial t)^2$. Figure 5b shows the variations of the Taylor microscale. The values of $\lambda$ in the drag wake are approximately twice those in the momentumless wake without swirl, but their radial distributions are similar in shape. The smallest values were measured in the isolated nonswirling jet (not shown), being almost half of those in the momentumless wake without swirl in the central part of the jet. The implications of these differences are not entirely clear as the Taylor microscale represents neither the dissipating scales not the larger eddies in the flow. The distribution of the Taylor microscale in the momentumless swirling wake is almost identical to that of the drag wake in the inner region of the flow up to approximately $r/b = 0.7$. The Taylor microscale is consistently larger for the swirling momentumless wake vs the nonswirling momentumless wake. The reason for this rather unexpected behavior is not clear.

## VI. Conclusions

Significant differences were found in quantities such as eddy viscosity, intermittency, triple velocity correlations, and turbulence length scales at the last measuring station in momentumless wakes, without and with swirl, and their respective component flows, i.e., drag wake and isolated jet without and with swirl. The implications of these differences with respect to turbulence modeling remain to be explored. The eddy viscosity in the momentumless wake with swirl is considerably smaller than in all of the other flows used for comparison, including the bare-body wake, the isolated swirling jet, and the momentumless wake without swirl. Measurements of the triple correlations do not reveal any consistent effect of swirl. The intermittency distribution in the three wakes (i.e., drag wake and both momentumless wakes with and without swirl) is similar. The two turbulence length scales show trends counter to those expected on the basis of similarity between both momentumless wakes.

## References

[1]Sirviente, A. I., and Patel, V. C., "Wake of a Self-Propelled Body, Part 1: Momentumless Wake," *AIAA Journal*, Vol. 38, No. 4, 2000, pp. 613–619.

[2]Sirviente, A. I., and Patel, V. C., "Wake of a Self-Propelled Body, Part 2: Momentumless Wake with Swirl," *AIAA Journal*, Vol. 38, No. 4, 2000, pp. 620–627.

[3]Sirviente, A. I., and Patel, V. C., "Experiments in the Turbulent Near Wake of an Axisymmetric Body," *AIAA Journal*, Vol. 37, No. 12, 1999, pp. 1670–1673.

[4]Tennekes, H., and Lumley, J. L., *A First Course in Turbulence*, MIT Press, Cambridge, MA, 1972.

[5]Lin, C. C., "On Taylor's Hypothesis and the Acceleration Terms in the Navier Stokes Equations," *Quarterly Applied Mathematics*, Vol. 10, No. 4, 1953, pp. 295–306.

R. M. C. So
*Associate Editor*

# Geometries for Five-Hole-Type Probes with Planar Sensor Arrays

H. Babinsky,* U. Kuschel,† H. P. Hodson,‡
D. F. Moore,§ and M. E. Welland¶
*Cambridge University, Cambridge, England CB2 1PZ, United Kingdom*

## Introduction

MANY of the most challenging problems of aerodynamics today are concerned with highly unsteady and three-dimensional flows. Examples can be found throughout turbomachinery, in transonic flows, and also in the research into turbulent structures. The study of such flowfields requires the measurement of velocity vectors at high spatial and frequency resolution. Although modern optical techniques can offer such features, their use is often limited by optical access, and a simpler pressure-based sensor would be preferable. Five-hole probes are widely used as a simple, robust, and useful tool for the determination of velocity vectors, but there is usually a tradeoff between their size and their frequency resolution.

Through the emergence of micro-electro-mechanical-systems (MEMS) technology[1,2] and its introduction into aeronautical sensor technology,[3] there are now good prospects to fabricate a five-hole probe, which is both small in size (<1 mm) and has the pressure sensors incorporated in the probe head itself to give a very high frequency response (>100 kHz). However, there are still very significant problems with this approach, in particular because MEMS technology has been developed from microelectronic fabrication processes, which are essentially planar systems. The complex three-dimensional shape of traditional five-hole probes does not lend itself easily to miniaturization.

Rediniotis and coworkers[4,5] have suggested ways to bypass this difficulty by manufacturing a planar array of five miniature pressure sensors mounted underneath a small hemisphere fitted with pressure holes connecting to the sensors. They have shown that, in principle, such an approach is feasible and could lead to a five-hole probe of approximately 1 mm diam with a high frequency response. The difficulties with this approach are that the hemisphere containing the tubes needs to be manufactured and assembled with the sensor array, thus limiting the minimum size achievable. Furthermore, the length and the small diameter of the connections between the pressure sensors and the relevant pressure tapping on the hemisphere surface have a deleterious effect on the response time.

Received 31 May 2000; revision received 23 March 2001; accepted for publication 20 July 2001. 

*Senior Lecturer in Aerodynamics, Department of Engineering, Trumpington Street. Member AIAA.

†Research Student, Department of Engineering, Trumpington Street.

‡Professor in Turbomachinery, Department of Engineering, Trumpington Street. Member AIAA.

§Lecturer in Electrical Engineering, Department of Engineering, Trumpington Street.

¶Professor in Electrical Engineering, Department of Engineering, Trumpington Street.